Chemistry–A European Journal
Research Article
doi.org/10.1002/chem.202500128
Chemistry Europe
European Chemical Societies Publishing
www.chemeurj.org

Unveiling the Dual Nature of the Smallest Aqueous Ferrocene Complex

Susana Blanco,[a] Andrés Verde,[a] Juan Carlos López,*[a] Manuel Yáñez,[b] M. Merced Montero-Campillo,[b] and Ibon Alkorta[c]

The structure of the ferrocene-water ($(Cp)_2Fe{:}H_2O$) complex has been characterized by combining state of the art rotational spectroscopy and computational chemistry. Two structures have been retrieved experimentally where water interacts with two distinguished binding sites, the *exo* Cp π cloud and the planetary-like planar orbit around iron. The spectra of both conformers exhibit significant averaging effects due to the nearly free rotational dynamics of water. This is in good agreement with the exploration of the potential energy surface of $(Cp)_2Fe{:}H_2O$. For water interacting with the *exo* Cp π cloud, we found three axial conformers giving rise to twenty minima with small internal rotation barriers. Theoretical calculations reveal two minima for the observed equatorial complex. Water interacts with ferrocene quite strongly, exhibiting binding energies above −11 kJ/mol in all binding sites and contributing to small deformations in the structure of bare ferrocene.

The discovery and subsequent elucidation of the structure of ferrocene ($Fe(\eta^5\text{-}C_5H_5)_2$, $(Cp)_2Fe$) resulted from the work of several research groups between 1951 and 1952.[1–4] Ferrocene has had a profound impact on organometallic chemistry, driving advancements in various fields, including catalysis, materials science, and medicinal chemistry.[5–8] Its versatile properties make it a valuable compound for both academic and industrial applications. The symmetry of ferrocene corresponds to the D_{5h} point group; consequently, it has no electric dipole moment, rendering it invisible to microwave spectroscopy. In contrast, several ferrocene derivatives have been successfully studied using this technique.[9–13] An alternative approach to making ferrocene detectable via rotational spectroscopy, which has not yet been explored, involves forming a complex with a molecule like water that possesses a permanent electric dipole moment. This can be achieved through supersonic jet expansion and subsequent analysis using microwave spectroscopy techniques.

Experimentally documented neutral complexes of unsubstituted ferrocene with small molecules are rare, and most of the available information is computational. Greenwald and collaborators investigated computationally $(Cp)_2Fe{:}CO$ complexes,[14] followed by studies on ferrocene complexes with N_2, O_2, H_2 and CH_4 at low temperature through IR spectroscopies.[15,16] Vrček and Bühl extensively studied ferrocene-containing alcohols through theoretical methods to explore the Fe···OH intramolecular interactions.[17] As part of this research, they also calculated equatorial ferrocene complexes with water, HF and CF_3OH, determining an interaction of $-5.02\ kJ\,mol^{-1}$ for the ferrocene-water complex. Ault has reported the ferrocene-HCl complex using DFT calculations and IR spectroscopy, characterizing hydrogen-bonded axial and equatorial complexes.[18] The investigation of binding sites on ferrocene has been of particular interest due to its protonation abilities,[19] and high proton affinity ($863.6\ kJ\,mol^{-1}$),[20] leading to studies of its complexes with H^+ or Li^+,[21–24] as well as simulations of the molecular dynamics of $FeCp_2H^+$.[25] Additionally, studies of the ferrocene dimer in the solid state revealed an isomer in which a hydrogen atom from one ferrocene unit points directly to the iron center of the neighboring ferrocene.[26,27] The role of hydrogen bonding in interactions with various transition metals has also been explored, highlighting the significance of studying such unusual interactions.[28–31]

In this context, the motivation for studying the ferrocene-water complex arises from several key considerations. First, such a complex provides a means of rendering ferrocene detectable in the gas phase through rotational spectroscopy, thereby overcoming the challenge posed by its lack of a permanent electric dipole moment. Second, water, as a proton donor, offers an opportunity to further explore the proton affinity of ferrocene, enhancing our understanding of its fundamental acid-base interactions. Finally, investigating the dynamics of water within the complex highlights the importance of moving beyond a purely static structural perspective when studying weakly bound complexes. This approach provides deeper insight into the nature of hydrogen bonding and intermolecular interactions in ferrocene-based systems, contributing to the broader understanding of organometallic solvation phenomena.

[a] *Prof. S. Blanco, A. Verde, Prof. J. C. López*
Departamento de Química Física y Química Inorgánica and IU-CINQUIMA, Facultad de Ciencias, Universidad de Valladolid, Valladolid, Spain
E-mail: juancarlos.lopeza@uva.es

[b] *Prof. M. Yáñez, Dr. M. M. Montero-Campillo*
Departamento de Química, Facultad de Ciencias, Universidad Autónoma de Madrid and Institute for Advanced Research in Chemical Sciences (IAdChem), Campus de Excelencia UAM-CSIC, Madrid, Cantoblanco 28049, Spain

[c] *Prof. I. Alkorta*
Instituto de Química Médica (CSIC), Juan de la Cierva, 3, 28006 Madrid, Spain

Supporting information for this article is available on the WWW under https://doi.org/10.1002/chem.202500128

Fourier-transform microwave (FTMW) spectroscopy, combined with supersonic jet expansions, enables the formation and stabilization of molecular complexes at low temperatures, allowing precise characterization of molecular geometries and intermolecular interactions. This technique offers high resolution and sensitivity, facilitating the detection of weakly bound species (see Experimental Details at the SI file). Quantum mechanical calculations complement these experiments by predicting stable structures, interaction energies, and spectroscopic signatures (see Computational Details at the SI file).[32,33] These insights aid in interpreting rotational spectra, optimizing experimental conditions, and distinguishing isomers. Moreover, quantum mechanical approaches enable the exploration of the dynamical behaviour of the complex, offering a deeper understanding of its intermolecular interactions.

The topology of the molecular electrostatic potential (MEP) of ferrocene (Figure 1) shows negative regions of $-81\ kJ\,mol^{-1}$ and $-32\ kJ\,mol^{-1}$ associated to the Cp rings and to five coplanar points equidistant to iron located in the middle of the sandwich. All the positive regions lie along the CH groups. This topology clearly indicates that potential hydrogen bonds from water are likely to form at either axial or equatorial binding sites.

Five conformers of the complex $(Cp)_2Fe{:}H_2O$ are obtained after a CREST[34] screening and posterior B3LYP–D3(BJ) and CCSD optimizations. Analysis of the complexes using the quantum theory of atoms in molecules (QTAIM)[35] leads to the molecular graphs (see Figure 2a) showing the bond paths (BP) and bond critical points (BCP) indicative of the existence of a bond or interaction. In complexes **A**(C_s)/**B**(C_s)/**C**(C_1) (axial forms) water is hydrogen bonded to the outer face of one of the cyclopentadienyl rings. The bond paths reveal that the interacting OH group is directed towards a carbon atom in **A** and towards the center of a C–C bond in **B**, while **C** represents an intermediate configuration.

However, although the remaining H from water is more distant, the reduced density gradient shown in the 3D-NCI plots[36,37] (Figure 2b) indicates the existence of a surface over the ring. This is attributed to a continuous weakly interacting region with the π cloud where the second hydrogen participates as well.

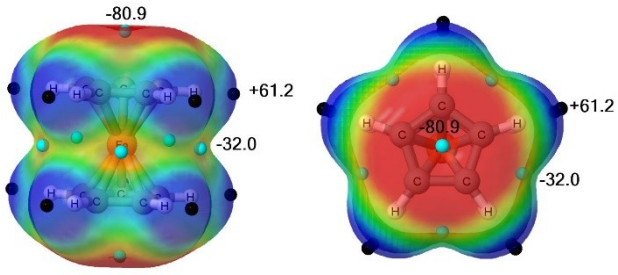

Figure 1. Side (left) and Top (right) views of the CCSD/def2-TZVP molecular electrostatic potential (MEP) of ferrocene on the 0.001 au electron density isosurface. Blue and red colors indicate regions with positive ($> +40$ kJ/mol) and negative (< -40 kJ/mol) values. Maxima and minima are indicated with black and light blue spheres.

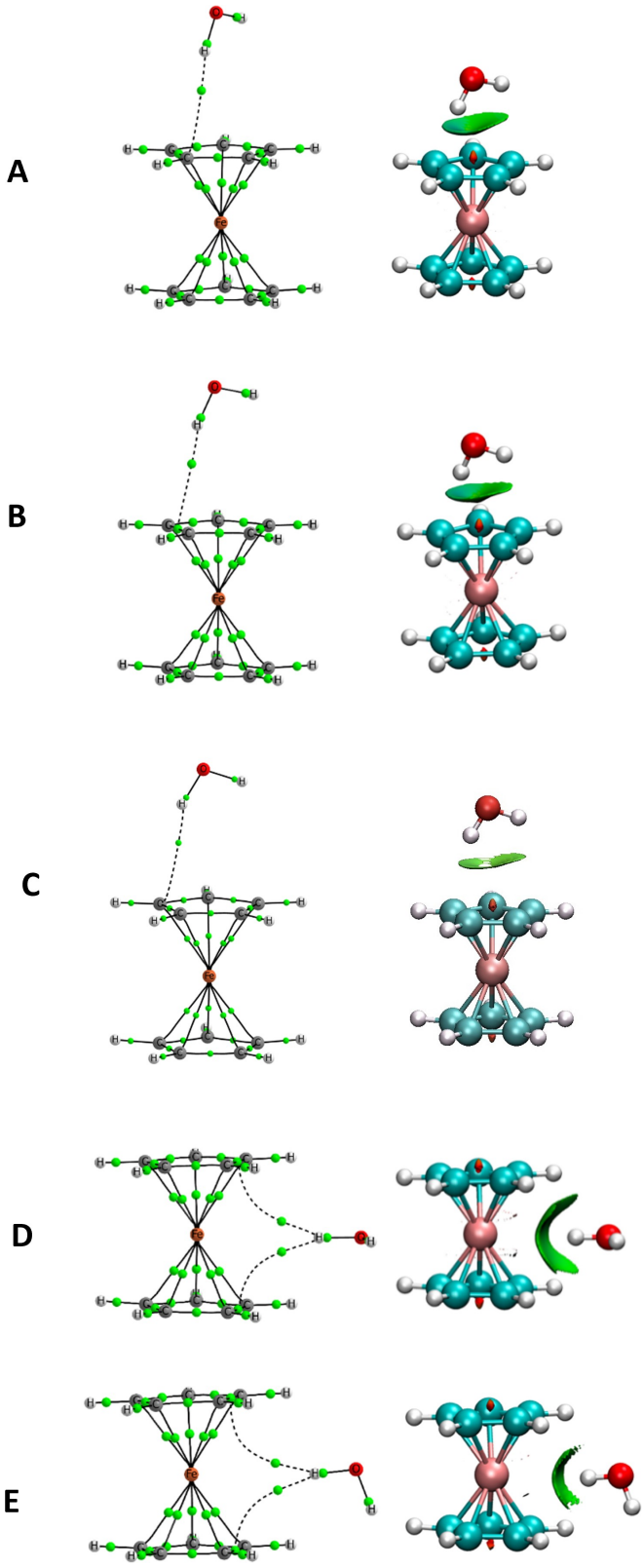

Figure 2. (a) First column: molecular graph of the five conformations obtained at CCSD/def2-TZVP computational level. Bond critical points are indicated with small green spheres. (b) Second column: 3D-NCI plots showing attractive weak NCIs in real space (green isosurfaces) and steric clashes from the rings (red color), RDG 0.4 a.u. See also 2D-plots in the SI file (Figure S7) for more info.

The potential energy surface (PES) has been investigated by a relaxed DFT scan along the coordinates of water's internal rotation, τ, and flipping motion, ϕ (Figure 3b). The internal rotation coordinate τ describes the dihedral angle between the water plane and one of the σ_v planes of ferrocene. Figure 3a shows the potential energy function $V(\tau)$ obtained from a relaxed scan along this coordinate revealing a total of 20 minima and 20 maxima with differences in energy of about 2 cm^{-1} (0.024 kJ mol^{1}). There are 5 equivalent minima located at 36°, 108°, 180°, 252°, and 324° corresponding to forms **A**, 5 equivalent minima at 0°, 72°, 144°, 216°, 288°, and 360°, corresponding to form **B** (the most stable form according to DFT calculations), and the remaining 10 equivalent minima, situated at intermediate positions between forms **A** and **B**, correspond to forms **C**. The interconversion between forms **A**, **B**, or **C** may also be done through the coordinate, ϕ, describing the water flipping motion. Figure 3c shows the potential energy function $V(\phi)$ connecting **A** and **B** forms, which is an asymmetric double minimum with a central barrier of 29 cm^{-1} at $\phi = 0°$ and minima at $\phi \sim 25°$. An estimation of the ground vibrational state for this motion from a reduced mass $\mu_\phi =$ 1.85 $uÅ^2$, calculated from the theoretical structure, shows it lies just above the barrier. Figure 3d shows the bidimensional PES profile along τ and ϕ coordinates describing a Mexican hat-like potential, with an almost isoenergetic path for water rotation. This results in a dynamic view of the intermolecular interactions as the rotation of water involves the rotation of the BPs and BCPs shown in Figure 2 for **A**/**B**/**C** forms around the cyclopentadienyl ring. In the complexes **D** and **E** (equatorial forms), the water molecule is located between the two cyclopentadienyl rings with one OH group pointing towards the iron atom. BCPs are indicative of the existence of a bond or interaction so their absence indicates that such an interaction does not exist. In fact, no BCP is observed between Fe and H but a simultaneous interaction of the OH hydrogen with the interstitial electron density between the water molecule and

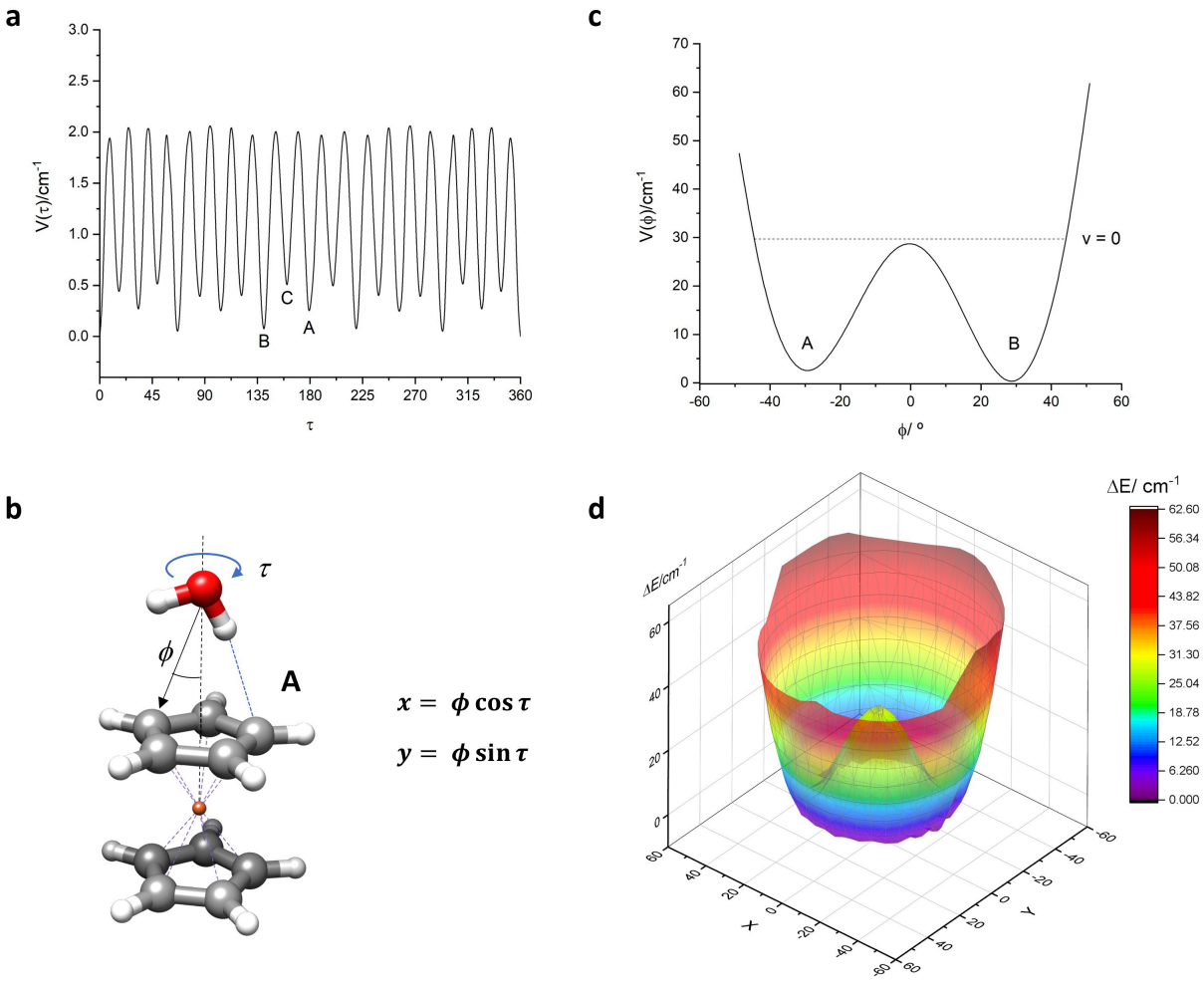

Figure 3. The results of the B3LYP-D3(BJ)/6-311 + + G(2d, p) exploration for the potential energy surface of $(Cp)_2Fe{:}H_2O$ for the axial complex in which water is linked to ferrocene on top of the cyclopentadienyl ring are summarized in this figure (see text). The results of a two-dimensional scan are also shown where the radial (ϕ) and angular (τ) coordinates have been transformed for convenience to the Cartesian coordinates *x* and *y* (second row on the right) and represented towards energy.

the rings, as evidenced by the curved isosurfaces within the weakly interacting region. The potential energy function for the rotation of water around the bonded O–H axis, interconverting **D** and **E** through a barrier lower than 20 cm $^{-1}$ (0.24 kJ mol^{-1}), is shown in Figure S1. The motion of water in the planetary-like orbit around iron gives a five-fold periodic potential function with barriers $V_5 \approx 6.0$ kJ mol^{-1}. The barriers between the **A**/**B**/**C** forms and **D**/**E** forms are so small that ground vibrational states are expected to lie above the barriers (Figures 3 and Figure S1). The binding energy of the five conformers is very similar at the three computational levels considered. At CCSD(T)//CCSD level with BSSE correction, it ranges between −12.2 kJ mol^{-1} and −11.3 kJ mol^{-1} (Table S1). The transition state configuration between the axial and equatorial forms calculated at B3LYP–D3(BJ)/Def2TZVP and MP2/Def2TZVP predicted to be at 8.2 kJ mol^{-1} and 10.1 kJ mol^{-1}, respectively, relative to the most stable axial forms is shown in Figure S2.

The rotational spectrum of the complex (Figure 4) is dominated by a series of evenly spaced doublet lines ($\Delta\nu \sim$ 1061.3 MHz) attributable to the successive J + 1←J transitions of a symmetric top. The rotational constant, $B \approx \Delta\nu/2$ ≈ 531 MHz, is close to the calculated constants for the axial $(Cp)_2Fe{:}H_2O$ forms (see Figure 4, Tables S2–S4). The observation of this complex as a symmetric top, although seemingly inconsistent with the symmetries of the calculated conformers, aligns with the predicted near-free rotation of water around the ferrocene C_5 symmetry axis (see Figure 3). This motion averages the *B* and *C* rotational constants into a single effective *B* value.

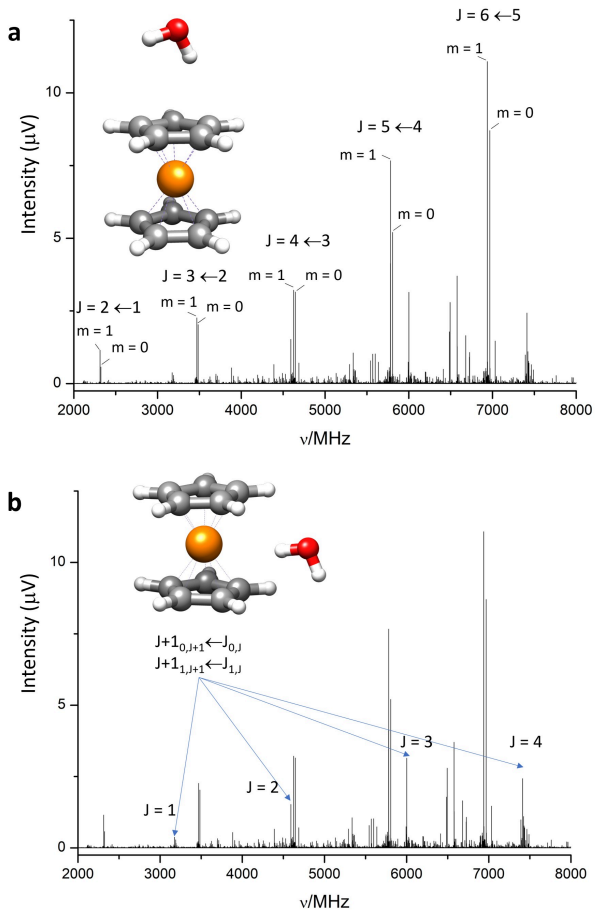

Figure 4. Rotational spectrum of a mixture of ferrocene and water in Ne recorded with a CP-FTMW spectrometer in the 2–8 GHz frequency region. **a**) The assignment of a symmetric rotor identified as the axial $(Cp)_2Fe{:}H_2O$ complex is shown. **b**) The assignment of an asymmetric top identified as the equatorial $(Cp)_2Fe{:}H_2O$ complex is shown.

Free rotation effects have been observed in complexes of water interacting with the π cloud of aromatic rings[38–40] or symmetric tops.[41] We have assigned the members of the doublets to the m = 0 and m = 1 free rotor quantum states (Figures 4 and Figure S3). In addition, *K* splittings caused by the centrifugal distortion constant D_{JK} (see Figure S3) are observed. Based on this assignment the spectrum was analysed according to:[42]

$$\nu_{J,K,m} = 2(J+1)(B - D_{JK}K^2 - D_{Jm}m^2) - 4D_J(J+1)^3 \quad (1)$$

from which the rotational parameters given in Table 1 were obtained. Alternatively, independent symmetric top semirigid rotor fits were done for each free rotation state (Table S5).

The equatorial forms of the $(Cp)_2Fe{:}H_2O$ complex (Figure 2 and Tables S2–S4) are oblate asymmetric tops with a dominant μ_a electric dipole moment component. Figure 4b shows the assignment of the spectrum of one of such conformers and the results of its analysis using the Watson[43] S-reduced Hamiltonian in the I^r representation are collected in Table 1.

The $^{54/57/58}$Fe and ^{13}C isotopologues of $(Cp)_2Fe{:}H_2O$ were observed in natural abundance. Isotopic substitution in the water subunit was investigated by using enriched D_2O and $H_2{}^{18}O$ samples. For the axial form (Figure S3) only two ^{13}C asymmetric rotor spectra were found with a ~5% relative intensity showing the equivalence of the carbon atoms for each Cp moiety. The *m* doublets observed for all species collapse into a single signal in the deuterated isotopologues, confirming that the origin of these doublets is associated with the internal rotation of water. For the equatorial form (Figure S4) three ^{13}C spectra with 2% (C_a), 4% (C_b) and 4% (C_c) relative intensities were observed. The rotational parameters for all observed species are given in Tables S5 and S6 and the observed frequencies in Tables S16–S45.

The structures of the complexes (Figure 5) were initially determined using the Kraitchman substitution method (r_s),[44,45] which directly provides the absolute coordinates of the substituted atoms. The sign of these coordinates can be taken from r_0 or r_e structures. The effective ground state, r_0, structure was obtained from a least-squares fit of all the available rotational parameters to determine the bond distances and angles.[46] A summary of the r_s, r_0, and r_e results for both the axial and equatorial forms of $(Cp)_2Fe{:}H_2O$ is presented in Figure 5. Detailed results are given in Tables S7–S15.

For the axial complex (Figure 5a), only the *a* coordinates could be determined. Exceptionally the *B* and *C* rotational constants of ^{13}C species allow a partial ferrocene r_0 structure determination using a centrosymmetric model. For the equatorial complex, there are two possible conformers, with the plane of water parallel or perpendicular to the aromatic ring planes

Table 1. Rotational parameters obtained from the fit of the rotational spectra of the axial and equatorial conformations of the complex $(Cp)_2Fe{:}H_2O$. The rotational constants are compared to the CCSD/def2-TZVP predicted values for the **A** and **D** conformers. The centrifugal distortion constants are compared to those calculated at B3LYP-D3(BJ)/def2-TZVP calculations.

	Axial		Equatorial	
Param.[a]	Exp.	CCSD (**A**)	Exp.	CCSD(**D**)
A/MHz	–	2196.8	1074.89428(70)	1076.7
B/MHz	580.65661(53)[b]	585.1	1059.30857(49)	1060.2
C/MHz	–	584.4	704.91214(28)	704.8
κ	−1.0	−0.9992	0.9157	0.9111
D_{Jm}/kHz	2.45258(37)			
D_J /kHz	0.0605(70)	0.046	[0.][c]	0.21
D_{JK}/kHz	2.842(25)	0.57	3.170(60)	−0.19
D_K /kHz		−0.57	−3.20(10)	0.033
d_1 /kHz		−0.00011	−0.0997(48)	0.049
d_2 /kHz		0.00011	−0.1471(37)	0.032
N	38		29	
σ /kHz	10.2		2.9	

[a] *A*, *B* and *C* are rotational constants; $\kappa = (2B\text{-}A\text{-}C)/(A\text{-}C)$ is the Ray's asymmetry parameter. D_{Jm}, D_J, D_{JK}, D_K, d_1, and d_2 are centrifugal distortion constants (see text for details); N is the number of lines fitted; σ is the standard deviation of the fit. [b] Standard error in parenthesis in units of the last digit. [c] Fixed to zero.

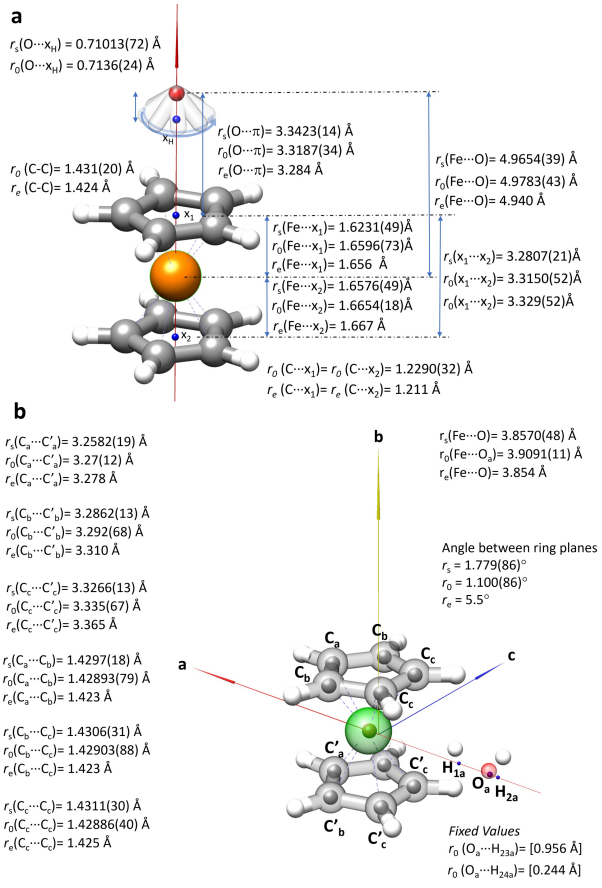

Figure 5. A summary of the r_s and r_0 structures of the $(Cp)_2Fe{:}H_2O$ complex and the comparison with the CCSD r_e theoretical structure for (a) the axial form, and (b) the equatorial form. For the equatorial form (b) the figure gives the r_s positions for the carbon and water atoms as spheres. The water r_0 *a* coordinates are presented as dots.

(see Figure 2). If we compare the r_s coordinates with the CCSD ones, there is only reasonable agreement for the parallel configuration. This arises (see Figure S6) because the rotation of water induces a rotation of the inertial axes system around *c* axis. Furthermore, the r_s data indicate a distorted water structure, with the oxygen atom and the bonded hydrogen atom positioned near the *a*-inertial axis, while the non-bonded hydrogen atom adopts a perpendicular arrangement (Figure 5b). The r_0-fitting of the rotational constants gives the worst results for a perpendicular arrangement of water and slightly better for a parallel arrangement, but none of these arrangements is consistent with the equivalences observed upon ^{13}C carbon substitutions, two equivalent C_a, four equivalent C_b, and four C_c atoms (see Figure 5b). A good result consistent with these equivalencies is obtained when considering that only the *a* coordinates of water atoms are determinable. The corresponding r_s and r_0 structures are compared in Figure 5b. Globally, the experimental data show a good consistency with the *ab initio* results and ferrocene electron diffraction structure.[47] Both theoretical and experimental data reflect the small distortion of the ferrocene structure due to the presence of water. In the axial form the distance between the ring centroid and the Fe nucleus is shorter for the interacting ring (Figure 5a). In the equatorial form the ring planes are not parallel, so the distance between equivalent carbon atoms is larger on the side in which ferrocene interacts with water (Figure 5b).

To characterize the nature of the interactions, we have analyzed the Laplacian of the electronic density ($\nabla^2\rho$), the electron density shift (EDS) and the DFT-SAPT energy decomposition analysis. The intermolecular BCPs shown in the molecular graphs (Figure 2) present small values of ρ (0.008–0.009 au), and positive values of $\nabla^2\rho$, typical of weak hydrogen

bonds. Charge transfer in hydrogen-bound systems is usually associated with an electric dipole moment enhancement. In this case, only for axial forms an increment of the total electric dipole moment of 0.66 D is observed, while in **D**/**E** no electric dipole moment enhancement is found (see Table S4). The calculation of the EDS (Figure 6) allows the visualization of the regions in space where charge has been lost or gained. The charge concentration region above the ring in forms **A**/**B**/**C** would be moving around as long as water rotates. It is also interesting to notice a charge concentration in a region intermediate between the O–H and the iron atom in **E**. These results agree with previous reports that have pointed out the possibility that metal atoms could act as HB acceptors.[28–31] Finally, the DFT-SAPT energy terms are gathered in Table 2. Note that the total DFT-SAPT energies are almost identical to the BSSE corrected CCSD(T) binding energies (Table S1), in line with the small deformation of the interacting molecules and the nice agreement between DFT and CCSD(T) methods. The absolute values for **D**/**E** are larger than for **A**/**B**/**C** for the different energy contributions: electrostatics, exchange, induction, and dispersion. Especially, the repulsive exchange term in **D** and **E** is 8 kJ/mol larger than in **A**/**B**/**C**, probably due to the proximity of the water molecule to the two cyclopentadienyl molecules. The electrostatic term is the dominant attractive component, contributing between 46% and 49%, followed by the dispersion term, which accounts for 37% to 39% of the total attractive interactions. The induction and δ(HF) terms have small attractive contributions (8 and 5%, respectively). The significance of exchange interactions in **D**/**E** results in a slightly more favorable global energy interaction in **A**/**B**/**C**.

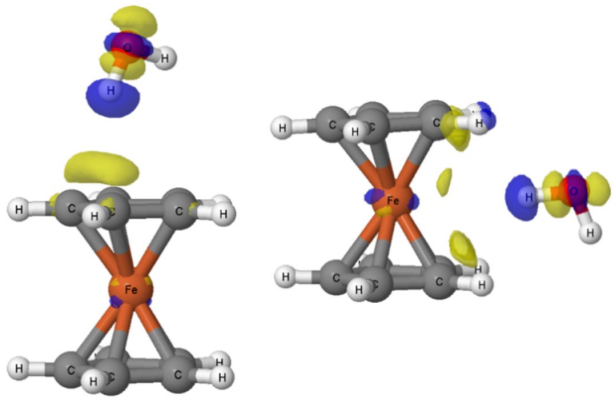

Figure 6. Electron density shifts of structures **B** (left) and **E** (right) calculated at CCSD/def2-TZVP level. Yellow and blue colors represent regions with gain and loss of charge (±0.001 au), respectively.

Table 2. Energy decomposition analysis carried out with DFT-SAPT showing the different contributions to the interaction energy in kJ mol^{-1}: E_{el} electrostatics, E_{ex} exchange, E_{ind} induction, E_{dis} dispersion, δ(HF) Hartree-Fock correction.

Conf	E_{el}	E_{ex}	E_{ind}	E_{dis}	δ(HF)	E_{SAPT}
A	−15.1	18.4	−2.7	−11.6	−1.5	−12.6
B	−15.1	18.5	−2.8	−11.6	−1.6	−12.6
C	−15.1	18.5	−2.8	−11.6	−1.6	−12.6
D	−18.3	27.2	−3.5	−14.7	−-2.0	−11.4
E	−17.5	26.8	−3.6	−14.9	−2.1	−11.2

Analysis of the $(Cp)_2Fe{:}H_2O$ complex by state-of-the-art rotational spectroscopy and computational chemistry methods allows us to conclude that this complex appears in the form of two almost isoenergetic species, where water interacts axially with the exo Cp π cloud or equatorially pointing to the iron atom. The quantum mechanical effects of water rotational dynamics prevent the experimental location of water hydrogen atoms. Both arrangements lead to binding energies above −11 kJ/mol, which are notably strong for a neutral complex of this nature. In both cases, experimental and theoretical data reveal minor deformations in the ferrocene structure caused by its interaction with water.

This study is significant as ferrocene lacks a permanent dipole, making its gas-phase detection challenging. Complexation with water enables structural characterization and provides insights into ferrocene's proton affinity. Interestingly, QTAIM analysis suggests that in equatorial conformers, the interaction involves electron density between Hand Cp rings rather than direct O–H···Fe bonding.

Furthermore, the analysis of water's dynamics underscores the importance of moving beyond a static structural perspective when studying weakly bound complexes. Understanding these dynamical effects provides a more complete picture of hydrogen bonding and intermolecular interactions in ferrocene systems, contributing to broader research on organometallic solvation, solubility, and reactivity. Insights into electron density redistribution further highlight the relevance of such studies for fundamental chemistry and potential applications in catalysis and materials science.

Supporting Information Summary

Complete experimental and theoretical details as well as additional figures and tables (43 pages, PDF). The authors have cited additional references within the Supporting Information (Ref. [48–65]).

Acknowledgements

This work was carried out with financial support from the projects PID2021-125207NB-C31, PID2021-125207NB-C32 and PID2021-125207NB-C33 of the Ministerio de Ciencia, Innovación y Universidades of Spain (MICINN). The authors also thank the Centro de Computación Científica of the UAM (CCC-UAM) for the generous allocation of computer time and continued technical support. SB, AV and JCL thank the Junta de Castilla y León (INFRARED-FEDER IR2020-1-UVa02) for research funds. A.V. would like to thank the University of Valladolid and Banco de Santander for his Ph.D. grant.

Conflict of Interests

The authors declare no conflict of interest.

Data Availability Statement

The data that support the findings of this study are available in the supplementary material of this article.

Keywords: Ferrocene · Microsolvation · Rotational spectroscopy · *Ab initio* · Noncovalent interactions

[1] T. J. Kealy, P. L. Paulson, *Nature* **1951**, *168*, 1039–1040.
[2] S. A. Miller, J. A. Tebboth, J. F. Tremaine, *J. Chem. Soc.* **1952**, 632–635.
[3] G. Wilkinson, M. Rosemblum, M. C. Whiting, *J. Am. Chem. Soc.* **1952**, *74*, 2125–2126.
[4] E. O. Fischer, W. Pfab, *Z. Naturforsch. B* **1952**, *7*, 377–379.
[5] P. Štěpnička, *Dalton Trans.* **2022**, *51*, 8085–8102.
[6] K. Heinze, H. Lang, *Organometallics* **2013**, *32*, 5623–5625.
[7] D. Astruc, *Eur. J. Inorg. Chem.* **2017**, *2017*, 6–29.
[8] R. K. Bohn, A. Haaland, *J. Organomet. Chem.* **1966**, *5*, 470–476.
[9] B. J. Drouin, T. G. Lavaty, P. A. Cassak, S. G. Kukolich, *J. Chem. Phys.* **1997**, *107*, 6541–6548.
[10] D. S. Margolis, C. Tanjaroon, S. G. Kukolich, *J. Chem. Phys.* **2002**, *117*, 3741–3747.
[11] R. Subramanlan, C. Karunatilaka, K. S. Keck, S. G. Kukolich, *Inorg. Chem.* **2005**, *44*, 3137–3145.
[12] R. Subramanian, C. Karunatilaka, R. O. Schock, B. J. Drouin, P. A. Cassak, S. G. Kukolich, *J. Chem. Phys.* **2005**, *123*, 054317.
[13] W. Sun, D. Kargin, Z. Kelemen, R. Pietschnig, M. Schnell, *ChemPhysChem* **2025**, *26*, e202400881.
[14] I. I. Greenwald, B. V. Lokshin, I. Abronin, V. Korsunov, N. Rudnevskii, *Bull. Acad. Sci. USSR Div. Chem. Sci. (Engl. Transl.)* **1986**, *35*, 2495–2497.
[15] B. V. Lokshin, I. I. Greenwald, *J. Mol. Struct.* **1990**, *222*, 11–20.
[16] I. I. Greenwald, B. V. Lokshin, N. Rudnevskii, V. M. Fomin, *Bull. Acad. Sci. USSR Div. Chem. Sci. (Engl. Transl.)* **1988**, *37*, 49–51.
[17] V. Vrček, M. Bühl, *Organometallics* **2006**, *25*, 358–367.
[18] B. S. Ault, *J. Phys. Chem. A* **2024**, *128*, 1233–1240.
[19] C. E. C. A. Hop, T. B. McMahon, *J. Am. Soc. Mass Spectrom.* **1994**, *5*, 274–281.
[20] E. P. L. Hunter, S. G. Lias, *J. Phys. Chem. Ref. Data* **1998**, *27*, 413–656.
[21] N. Sharma, J. K. Ajay, K. Venkatasubbaiah, U. Lourderaj, *Phys. Chem. Chem. Phys.* **2015**, *17*, 22204–22209.
[22] M. J. Mayor-López, J. Weber, B. Mannfors, A. F. Cunningham, *Organometallics* **1998**, *17*, 4983–4991.
[23] A. Irigoras, J. M. Mercero, I. Silanes, J. M. Ugalde, *J. Am. Chem. Soc.* **2001**, *123*, 5040–5043.
[24] J. Rodríguez-Otero, E. M. Cabaleiro-Lago, A. Peña-Gallego, M. M. Montero-Campillo, *Tetrahedron* **2009**, *65*, 2368–2371.
[25] M. Bühl, S. Grigoleit, *Organometallics* **2005**, *24*, 1516–1527.
[26] F. H. Allen, *Acta Crystallogr. Sect. B* **2002**, *58*, 380–388.
[27] A. Vargas-Caamal, S. Pan, F. Ortiz-Chi, J. L. Cabellos, R. A. Boto, J. Contreras-García, A. Restrepo, P. K. Chattaraj, G. Merino, *Phys. Chem. Chem. Phys.* **2016**, *18*, 550–556.
[28] I. Alkorta, I. Rozas, J. Elguero, *J. Mol. Struct.* **2001**, *537*, 139–150.
[29] L. Brammer, J. M. Charnock, P. L. Goggin, R. J. Goodfellow, A. G. Orpen, T. F. Koetzle, *J. Chem. Soc. Dalton Trans.* **1991**, 1789–1798.
[30] L. Brammer, *J. Chem. Soc. Dalton Trans.* **2003**, 3145–3157.
[31] E. Andris, M. Straka, J. Vrána, A. Růžička, J. Roithová, L. Rulíšek, *Chem. Eur. J.* **2023**, *29*, e202203769.
[32] M. J. Frisch, *et al.*, *Gaussian 16 Rev. A.03*, Wallingford, CT **2016**.
[33] H.-J. Werner, P. J. Knowles, G. Knizia, F. R. Manby, M. Schütz, *WIREs Comput. Mol. Sci.* **2012**, *2*, 242–253.
[34] P. Pracht, F. Bohle, S. Grimme, *Phys. Chem. Chem. Phys.* **2020**, *22*, 7169–7192.
[35] R. F. W. Bader, *Acc. Chem. Res.* **1985**, *18*, 9–15.
[36] E. R. Johnson, S. Keinan, P. Mori-Sánchez, J. Contreras-García, A. J. Cohen, W. Yang, *J. Am. Chem. Soc.* **2010**, *132* (18), 6498–6506.
[37] T. Lu, F. Chen, *J. Comput. Chem.* **2012**, *3*, 580–592.
[38] E. Arunan, T. Emilsson, H. S. Gutowsky, *J. Chem. Phys.* **1993**, *99*, 6208–6210.
[39] P. Halder, M. S. Krishnan, E. Arunan, *J. Mol. Spectrosc.* **2020**, *370*, 111277.
[40] L. Evangelisti, K. Brendel, H. Mäder, W. Caminati, S. Melandri, *Angew. Chem. Int. Ed.* **2017**, *56*, 13699–13703.
[41] S. Blanco, A. Macario, J. García-Calvo, A. Revilla-Cuesta, T. Torroba, J. C. López, *Chem. Eur. J.* **2021**, *27*, 1680–1687.
[42] G. T. Fraser, F. J. Lovas, R. D. Suenram, D. D. Nelson, W. Klemperer, *J. Chem. Phys.* **1986**, *84*, 5983–5988.
[43] J. K. G. Watson, in *Vibrational Spectra and Structure a Series of Advances*, Vol. 6, (Ed.: J. R. Durig), Elsevier, New York **1977**; pp 1–89.
[44] J. Kraitchman, *Am. J. Phys.* **1953**, *21*, 17–24.
[45] B. P. van Eijck, *J. Mol. Spectrosc.* **1982**, *91*, 348–362.
[46] Z. Kisiel, *J. Mol. Spectrosc.* **2003**, *218*, 58–67.
[47] A. Haaland, J. E. Nilsson, *Acta Chem. Scand.* **1966**, *22*, 2653–2670.

Manuscript received: January 13, 2025
Accepted manuscript online: February 24, 2025
Version of record online: March 7, 2025